Eur. Phys. J. C (2025) 85:719
https://doi.org/10.1140/epjc/s10052-025-14434-0

THE EUROPEAN PHYSICAL JOURNAL C

Regular Article - Theoretical Physics

# Quantum effects on greybody factor via quantum Oppenheimer–Snyder-dS spacetime

**Zhiwei Lv**[1,a], **Sulaman Shaukat**[2,b], **Orhan Donmez**[3,c], **Faisal Javed**[4,5,d], **Arfa Waseem**[6,e]

[1] Department of Mathematics, Suqian University, Suqian 223800, China
[2] Department of Mathematics, University of the Punjab, Quaid-e-Azam Campus, Lahore 54590, Pakistan
[3] College of Engineering and Technology, American University of the Middle East, Egaila 54200, Kuwait
[4] Department of Physics, Zhejiang Normal University, Jinhua 321004, People's Republic of China
[5] Research Center of Astrophysics and Cosmology, Khazar University, 41 Mehseti Street, AZ1096 Baku, Azerbaijan
[6] Department of Mathematics, Government College Women University, Sialkot, Pakistan

Received: 1 March 2025 / Accepted: 15 June 2025


**Abstract** The greybody factor of quantum Oppenheimer–Snyder-de Sitter spacetime is examined in this study. We determined the effective potential and examined its role under several physical factors, such as mass, rotational momentum, and quantum parameters, by transforming the Klein–Gordon equation into a Schrödinger-like wave equation through tortoise coordinates. Our results show that the absorption and scattering of massless scalar fields are strongly affected by the decrease in the effective potential caused by an increase in the quantum parameter. It is observed that the appearance of the quantum factor significantly increases the Schwarzschild–de Sitter black hole's effective potential. We discovered that waves behave differently at the event horizon, with lower-frequency waves bouncing off possible impediments and higher-frequency waves more readily penetrating them. Our investigation of the greybody component further demonstrates the significance of effective potential in wave transmission and reflection, demonstrating a substantial link between wave frequency and emission rates. In order to understand particle behavior at black hole horizons, it is shown that higher-frequency waves are more likely to pass through potential barriers, whereas lower-frequency waves prefer to reflect. This study advances our understanding of quantum field theory in curved spacetime and black hole thermodynamics, particularly in relation to scalar field interactions with black holes.

[a] e-mail: sdlllzw@mail.ustc.edu.cn
[b] e-mail: sulamanshaukat444@gmail.com
[c] e-mail: orhan.donmez@aum.edu.kw
[d] e-mail: faisaljaved.math@gmail.com (corresponding author)
[e] e-mail: arfa.waseem@gcwus.edu.pk (corresponding author)

## 1 Introduction

Researchers have been captivated by the study of black holes (BHs) for many years because of their deep gravitational properties, but their relevance goes beyond simple gravitational events. It is often accepted that understanding thermodynamic principles in the most severe circumstances of the cosmos requires an understanding of BHs. Black hole thermodynamics is an interdisciplinary field that combines quantum physics, general relativity, and classical thermodynamics. It has grown to be an important and fascinating area of research. Our understanding of BH dynamics is improved, and it could also serve as a means of advancing the unified theory of quantum gravity. A key characteristic of BHs is their event horizon. When particles approach the border, they are drawn into the BH. Bekenstein's fundamental theory that BHs must have entropy [1] was the basis for BH thermodynamics. His study found a direct relationship between the entropy of a BH and the area of its event horizon, indicating that the horizon's surface area may be used as a gauge for the disorder or informational content of a BH. The scientific view of BHs was transformed by this idea, which saw them as thermodynamic systems that follow concepts similar to classical thermodynamics rather than just being objects that absorb matter and energy. In the context of loop quantum theory, Lewandowski et al. [2] have recently put out a novel quantum BH model. This model uses a properly distorted Schwarzschild BH as its external spacetime. Using the effective corrections in loop quantum BHs, Lin and Zhang [3] obtained a cosmological constant-containing 4-dimensional spherically symmetric metric. They obtained the equations of motion by applying the holonomy corrections to the compo-

Published online: 01 July 2025

nents of Ashtekar variables in classical theory and imposing the areal gauge. By solving these equations, they obtained the formula for the effective metric in Painlevé–Gullstrand coordinates. In a surprising deviation from the conventional model, they discovered that, for a small BH, the loop quantum gravity BH's temperature drops as mass drops [3]. According to the study of quasi-normal modes, this quantum corrected BH is stable against test scalar and vector fields and has the same asymptotic behavior as the Schwarzschild BH [4]. The solution describing a quantum BH with a cosmological constant is found in [5] using a similar technique. Although the BH shadow of this spacetime has been the subject of several researches, a generalization of the spherically symmetric solution to rotating BH solution utilizing the well-known Newman–Janis method [6] is required to comply with experimental testing. Further, the detailed analysis of BH shadows in the framework of quantum Oppenheimer–Snyder spacetime with cosmological constant is presented in [7]. Various researchers observed the different properties of well-known quantum BHs [8,9,11**?** –16].

In 1974, Stephen Hawking made a major discovery by demonstrating that BHs could emit radiation, which is known as Hawking radiation, based on Bekenstein's work. This radiation is the result of quantum mechanical processes near the event horizon, where pairs of particles and antiparticles are created, one of which escapes and the other is absorbed by the BH. This process finally causes the BH to lose mass and evaporate [17]. By connecting BH thermodynamics and quantum mechanics, Hawking's finding challenged the prevalent understanding of BHs as entities from which nothing can escape. These results increased the complexity of BHs' thermodynamic properties by revealing that their temperature is limited and associated with their mass and surface area [18]. Currently, Bekenstein and Hawking's discovery of the relationship between an event horizon's area and entropy is considered essential to BH thermodynamics. The four rules of BH thermodynamics, which are quite identical to the classical thermodynamical laws, were clarified by their cooperation. These principles regulate the behavior of BH systems concerning temperature, entropy, and energy conservation [19]. The second law of BH thermodynamics, which asserts that a BH's total entropy cannot diminish, parallels the second law of thermodynamics, which stipulates that the total entropy of a closed system remains non-decreasing.

Recent investigations indicate a robust correlation between BHs and thermodynamic systems [20–22]. One may get significant insights into quantum gravity by resolving Einstein's field equations and treating BHs as thermodynamic systems characterized by entropy and heat [23–25]. The possible relationship between the generalized Born–Infeld scenario and string theory was examined in [26]. The negative cosmic constant is seen as a fluctuating thermodynamic pressure for BH over the extended phase space. The BH mass is viewed as the enthalpy of spacetime instead of its internal energy, while the conjugate variable in anti-de Sitter (dS) BH physics indicates the volume of the BH [27]. Using Lovelock theory, researchers examined AdS BHs in a specific framework [28]. Reference [29] outlines the precise formulae for the mass as well as the free energy of AdS BHs in the framework of Lovelock gravity. Additionally, according to the research of dilaton-AdS BHs, the enthalpy of the BH is analogous to its mass [30]. This substantial research yielded essential consequences in the thermodynamic analysis of AdS BHs in the extended phase space. The thermodynamic characteristics of several systems have been elucidated by contrasting BH models [31,32] with the dynamics of van der Waals fluids [33–35]. The AdS and CFT exhibit a profound connection as shown by the parallels identified between BHs in AdS space [36]. The frequency of the emission rate near the position of the horizon can be described by [17]

$$\gamma(w) = \left( \frac{d^3k}{e^{\frac{w}{T_H}} (2\pi)^3} \right).$$

The variable $d^3k$ represents a change in surface gravity, $w$ indicates the frequency, and $T_H$ represents the Hawking temperature in this equation. Both massive and massless particles may be described by this equation, which can be applied to any spatial dimension. The radiation spectrum at the event horizon seems to be a black body, which contributes to the information loss problem. The curvature of spacetime surrounding a BH affects the Hawking radiation spectrum, causing some radiation to depart and some to return to the BH. The probability of absorption of an incoming wave from infinity by the BH is measured by the absorption probability rate, also called the greybody factor (GBF). According to references [37–41], there is a substantial correlation between this component and the absorption cross-section. The association between the GBF and the emission rate could be represented mathematically as [37–41]:

$$\gamma(w) = \left( \frac{|A_{l,m}|^2 d^3k}{e^{\frac{w}{T_H}} (2\pi)^3} \right),$$

where GBF, a quantity that is dependent on frequency, is provided as $|A_{l,m}|^2$.

The research work presented in this article is devoted to exploring the GBF of quantum Oppenheimer Snyder–de Sitter-dS spacetime. The article is structured as follows: in Sect. 2, we discuss the quantum Oppenheimer Snyder-dS spacetime, focusing on the study of Klein–Gordon equations and the effective potential with the presence of the massless scalar field. We also derive an effective potential function from the radial equation of motion (EoM). We obtain the

analytical solutions through the radial EoM for both near as well as faraway horizons in Sect. 3. We then match these solutions in Sect. 4 and obtain the respective expressions for the rate of absorption as well as the emission of massless scalar fields. We present some outcomes of the presented analysis in the last section.

## 2 Quantum Oppenheimer Snyder-dS spacetime and Klein–Gordon equation

We consider a spherically symmetric metric ansatz [5,7]

$$ds^2 = -f(r)dt^2+(f(r))^{-1}dr^2+r^2d\theta^2+r^2\sin^2\theta d\phi^2, \quad (1)$$

having

$$f(r) = \frac{1}{r^4}\left(\alpha M^2\right)\left(\frac{\Lambda r^3}{6M}+1\right)^2 - \frac{2M}{r} - \frac{\Lambda r^2}{3} + 1, \quad (2)$$

here mass of BH is specified by $M$ while $\alpha$ denotes the quantum factor, and $\Lambda$ is a cosmological constant. Here, we analytically evaluate the GBF. Initially, we evaluate the EoM to examine the propagation of a massless scalar field. It is believed that particles have no additional connections and are only weakly related to gravity. In this context, the equation of motion in curved spacetime is expressed as the Klein–Gordon equation:

$$\frac{1}{\sqrt{-g}}\partial_\beta[\sqrt{-g}g^{\beta\gamma}\partial_\gamma\Psi] = 0, \quad (3)$$

having the massless scalar field $\Psi = \Psi(t, r, \theta, \phi)$. From Eq. (1), it is found that

$$\frac{-r^2\sin\theta}{f(r)}\partial_{tt}\Psi + \sin\theta\partial_r\left(r^2f(r)\partial_r\Psi\right) + \partial_\theta\left(\sin\theta\partial_\theta\Psi\right) + \frac{1}{\sin\theta}\partial_{\phi\phi}\Psi = 0. \quad (4)$$

The technique of separation of variables allows one to attain

$$\Psi = \exp(-\iota w t)\exp(\iota m\phi)R_{wlm}(r)Q_l^m(\theta, aw), \quad (5)$$

with the angular spheroidal function $Q_l^m(\theta, aw)$. Equation (4) yields the expressions of the radial as well as the angular constituents of the EoM as [42,43]

$$\frac{\partial}{\partial r}\left[r^2f(r)\frac{\partial R_{wlm}}{\partial r}\right] + \left[\frac{r^2\omega^2}{f(r)} - \lambda_l^m\right]R_{wlm}(r) = 0, \quad (6)$$

and

$$\frac{\partial}{\partial\theta}\left[\sin\theta\frac{\partial Q_l^m}{\partial\theta}\right] + \left[\frac{-m^2}{\sin\theta} + \lambda_l^m\sin\theta\right]Q_l^m(\theta, aw) = 0, \quad (7)$$

respectively. The relationship between the decoupled equations is displayed by the separation constant $\lambda_l^m = l^2 + l$ [42,43]. We may investigate the effective potential that explains the GBF by resolving the previously mentioned radial equation. A novel radial transformation is specified as

$$R_{wlm}(r) = \frac{U_{wlm}(r)}{r}. \quad (8)$$

With the help of tortoise component $x_*$, we obtain

$$\frac{dx_*}{dr} = \frac{1}{f(r)}, \quad (9)$$

providing

$$\frac{d}{dx_*} = f(r)\frac{d}{dr}, \quad (10)$$

$$\frac{d^2}{dx_*^2} = f^2(r)\frac{d^2}{dr^2} + ff'\frac{d}{dr}. \quad (11)$$

$x_* \to -\infty$ when $r$ approaches to the BH horizon radius ($r_h$), and $x_* \to \infty$ for $r \to \infty$. In comparison to Eq.(6), which is restricted to a location distant from the BH horizon, the system's range with the tortoise coordinates $x_*$ varies from $-\infty$ to $+\infty$. Equation (6) is characterized by a Schrödinger wave equation, presented as

$$\left(\frac{d^2}{dx_*^2} - V_{eff}\right)U_{wlm}(r) = 0. \quad (12)$$

The associated form of the effective potential becomes

$$V_{eff} = -\omega^2 + \frac{ff'}{r} + \frac{\lambda_l^m f(r)}{r^2}.$$

For several choices of BH parameters, we have observed the behavior of effective potential as shown in Figs. 1 and 2. Figs. 1 and 2 shows the role of BH's mass, angular momentum, and quantum parameter on the effective potential. As seen in Fig. 1, a greater peak in the potential function is the result of smaller choices of the quantum factor $\alpha$. In contrast, as seen in Fig. 2, an increase in the mass of BH reduces the effective potential while effective potential increases by increasing the angular momentum. These findings suggest that the quantum parameter greatly affects the behavior of the effective potential of the considered manifold.

## 3 Greybody factor

In this section, we compute the analytic expression of GBF by solving the radial EoM. We solve Eq. (6) for two asymptotic regions separately, i.e., close to the BH horizon and far away from it. These two solutions will be extended and matched

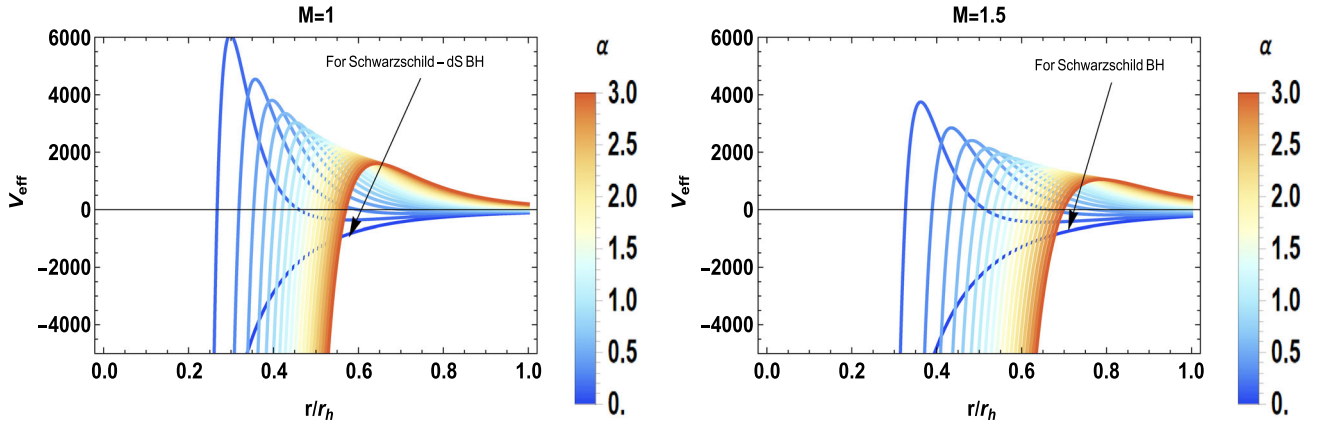


**Fig. 1** $V_{eff}$ versus $r/r_h$ by varying $\alpha$ and $\beta$ with $M$ with $l = 10$, $\omega = 2$, $\Lambda = 0.002$

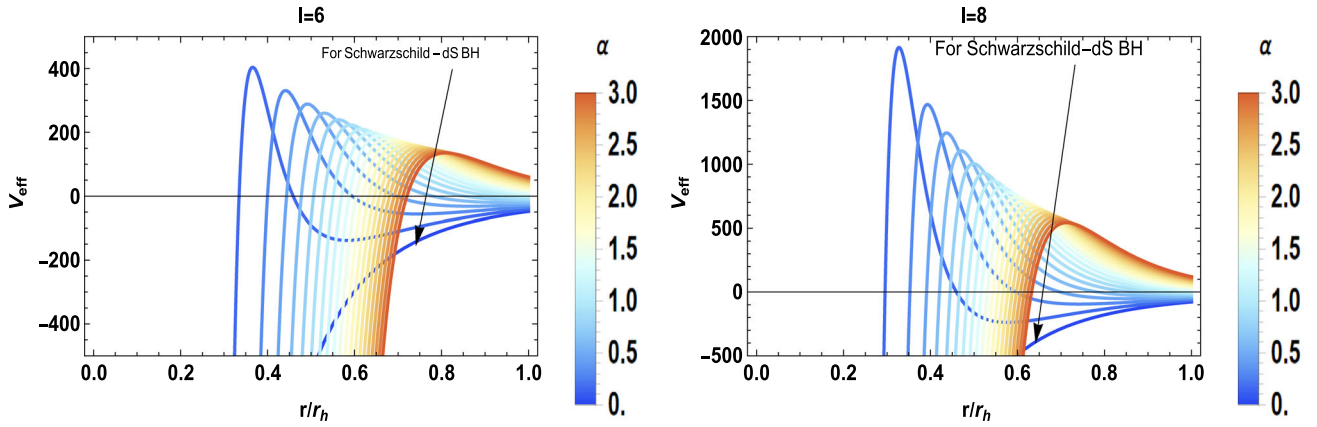


**Fig. 2** $V_{eff}$ versus $r/r_h$ by varying $\alpha$ and $L$ with $M = 1$, $\omega = 2$, $\Lambda = 0.002$

smoothly in an intermediate region to obtain the analytical expression for the whole radial domain. The exact solution for the near horizon domain $r \sim r_h$ is obtained by using the following transformation:

$$r \to S = \frac{1 - \frac{2M}{r} - \frac{\Lambda r^2}{3} + \frac{\alpha M^2}{r^4}\left[1 + \frac{\Lambda r^3}{6M}\right]^2}{1 - \frac{\Lambda r^2}{3}}, \tag{13}$$

which yields

$$\frac{dS}{dr} = \frac{(1-S)U(r_h)}{r_h},$$

also, we have

$$U(r_h) = r_h\left[\frac{P'}{P} - \frac{O'}{O}\right], \quad P(r_h) = 1 - \frac{\Lambda r_h^2}{3},$$
$$O(r_h) = -\frac{2M}{r_h} + \frac{\alpha M^2}{r_h^4}\left[1 + \frac{\Lambda r_h^3}{6M}\right]^2$$

The radial equation (6) associated with the above outcomes can be presented by

$$S(1-S)\frac{d^2R_{wlm}}{dS^2} + (A - BS)\frac{dR_{wlm}}{dS} + \frac{1}{(1-S)U^2}\left[\frac{\chi_h}{S} - \lambda_h\right]R_{wlm} = 0, \tag{14}$$

where

$$A = \frac{r_h}{(1-S)U(r_h)}\frac{d}{dr}(S - S^2),$$
$$B = -\frac{S}{U^2(r_h)\left(1 - \frac{\Lambda r_h^2}{3}\right)}\frac{d}{dr}\left[r_h U(r_h)\left(1 - \frac{\Lambda r_h^2}{3}\right)\right],$$
$$\chi_h = \frac{w^2 r_h^2}{\left(1 - \frac{\Lambda r_h^2}{3}\right)^2}, \quad \lambda_h = \frac{\lambda_l^m}{1 - \frac{\Lambda r_h^2}{3}},$$

The function in Eq. (14) is re-written as

$$R_{wlm}(S) = S^{\epsilon_1}(1-S)^{\eta_1}\hat{F}(S). \tag{15}$$

The following expression of Eq. (14) is then attained:

$$S(1-S)\frac{d^2\hat{F}(S)}{dS^2}+\left[2\epsilon_1+A-(2\epsilon_1+2\eta_1+B)S\right]\times\frac{d\hat{F}(S)}{dS}+\left[\left(\epsilon_1^2-\epsilon_1+A\epsilon_1+\frac{\chi_h}{U^2}\right)\frac{1}{S}+\left(\eta_1^2-\eta_1-\eta_1A+\eta_1B+\frac{\chi_h}{U^2}-\frac{\lambda_h}{U^2}\right)\frac{1}{1-S}\right]\hat{F}(S)=0. \tag{16}$$

We may compute the power coefficients $\epsilon_1$ as well as $\eta_1$ via

$$\epsilon_1^2-\epsilon_1+A\epsilon_1+\frac{\chi_h}{U^2}=0,$$
$$\eta_1^2-\eta_1-\eta_1A+\eta_1B+\frac{\chi_h}{U^2}-\frac{\lambda_h}{U^2}=0.$$

Thus, the solution of Eq. (16) provides the hypergeometric (HG) gradient equation as

$$S(1-S)\frac{d^2\hat{F}(S)}{dS^2}+\left[\bar{c}_1-(\bar{a}_1+\bar{b}_1+1)S\right]\frac{d\hat{F}(S)}{dS}-\bar{a}_1\bar{b}_1\hat{F}(S)=0, \tag{17}$$

with

$$\bar{a}_1=\eta_1+\epsilon_1+B-1,\quad \bar{b}_1=\eta_1+\epsilon_1,\quad \bar{c}_1=2\epsilon_1+A.$$

For the NH, its general solution is displayed by

$$(R_{wlm})_{NH}(S)=\hat{A}_1S^{\epsilon_1}(1-S)^{\eta_1}\hat{F}(\bar{a}_1,\bar{b}_1,\bar{c}_1;S)+\hat{A}_2S^{-\epsilon_1}(1-S)^{\eta_1}\hat{F}(1-\bar{c}_1+\bar{a}_1,1+\bar{b}_1-\bar{c}_1,-\bar{c}_1+2;S), \tag{18}$$

in which $\hat{A}_1$ and $\hat{A}_2$ are constants possessing

$$\epsilon_1^{\pm}=\frac{1}{2}\left[(1-A)\pm\sqrt{(1-A)^2-4\frac{\chi_h}{U^2}}\right],$$
$$\eta_1^{\pm}=\frac{1}{2}\left[(1+A-B)\pm\sqrt{(1+A-B)^2+4\left(\frac{\lambda_h}{U^2}-\frac{\chi_h}{U^2}\right)}\right].$$

Applying the boundary limits, we found that the BH horizon has no outward modes. $\hat{A}_1=0$ is an option; if not, $\hat{A}_2=0$. The selection of $\epsilon_1$ is necessary for this. By setting $\hat{A}_2=0$, we can prove that $\epsilon_1^+=\epsilon_1^-$ since $\hat{A}_1$ and $\hat{A}_2$ are constants for both values of $\epsilon_1$. The HG function's convergence condition that holds for $\eta_1^+=\eta_1^-$, can be employed as well to find the signs of $\eta_1$. Thus, the analytic form of the NH is seen as

$$(R_{wlm})_{NH}(S)=\hat{A}_1S^{\epsilon_1}(1-S)^{\eta_1}\hat{F}(\bar{a}_1,\bar{b}_1,\bar{c}_1;S). \tag{19}$$

We employ the identical technique as for NH to get the solution of the radial equation corresponding to the far BH horizon by inserting $T(r)$ instead of $f(r)$.

$$T(r)=\frac{1-\frac{\Lambda r^2}{3}}{r^2}. \tag{20}$$

Thus, the radial equation becomes

$$T(1-T)\frac{d^2R_{wlm}}{dT^2}+(C-D^*T)\frac{dR_{wlm}}{dT}+\frac{1}{D^2(1-T)}\left[\frac{\chi_f}{T}-\lambda_f\right]R_{wlm}=0,$$

where

$$\chi_f=\left(\frac{rwT(1-T)}{f(r)}\right)^2,\quad \lambda_f=\frac{\lambda_l^mT(1-T)^2}{f(r)},$$
$$C=\frac{1-\frac{\Lambda r^2}{3}}{rD^2f(r)}\frac{d}{dr}\left[Df(r)\right],\quad D^*=\frac{1-\frac{\Lambda r^2}{3}}{r^2D},$$
$$D=\frac{-2}{r^2}.$$

The expression in the previously described gradient equation needs to be re-expressed as

$$R_{wlm}(T)=T^{\epsilon_2}(1-T)^{\eta_2}F(\hat{T}), \tag{21}$$

we get

$$T(1-T)\frac{d^2F(\hat{T})}{dT^2}+\left[2\epsilon_2+C-(2\epsilon_2+2\eta_2+D^*)T\right]\frac{dF(\hat{T})}{dT}+\left[\left(\epsilon_2^2-\epsilon_2+\epsilon_2C+\frac{\chi_f}{D^2}\right)\times\left(\eta_2^2-\eta_2-\eta_2C+\eta_2D^*+\frac{\chi_f}{D^2}-\frac{\lambda_f}{D^2}\right)\frac{1}{1-T}\right]\times F(\hat{T})=0.$$

The power coefficients $\epsilon_2$ and $\eta_2$ become

$$\epsilon_2^2-(1-C)\epsilon_2+\frac{\chi_f}{D^2}=0,$$
$$\eta_2^2-(1-D^*+C)\eta_2+\frac{\chi_f}{D^2}-\frac{\lambda_f}{D^2}=0.$$

The equation based on HG is evaluated as

$$\bar{a}_2=-1+\epsilon_2+D^*+\eta_2,\quad \bar{b}_2=\eta_2+\epsilon_2,\quad \bar{c}_2=2\epsilon_2+C,$$

which gives

$$T(1-T)\frac{d^2F(\hat{T})}{dT^2}+\left[\bar{c}_2-(1+\bar{a}_2+\bar{b}_2)\right]\frac{dF(\hat{T})}{dT}-\bar{a}_2\bar{b}_2F(\hat{T})=0.$$

The general solution is

$$(R_{wlm})_f(T)=\hat{B}_1T^{\epsilon_2}(1-T)^{\eta_2}\hat{F}(\bar{a}_2,\bar{b}_2,\bar{c}_2;T)+\hat{B}_2T^{-\epsilon_2}(-T+1)^{\eta_2}\hat{F}(1-\bar{c}_2+\bar{a}_2,1-\bar{c}_2+\bar{b}_2,-\bar{c}_2+2;T), \tag{22}$$

having

$$\epsilon_2^{\pm} = \frac{1}{2}\Bigg[(1-C) \pm \sqrt{(1-C)^2 - 4\frac{\chi_f}{D^2}}\Bigg],$$
$$\eta_2^{\pm} = \frac{1}{2}\Bigg[(1+C-D^*) \pm \sqrt{(1+C-D^*)^2 - 4\left(\frac{\chi_f}{D^2} - \frac{\lambda_f}{D^2}\right)}\Bigg],$$

where the constants $\hat{B}_1$ and $\hat{B}_2$ are selected randomly. Identical to NH, we use the HG convergence constraint to obtain the results, where $\epsilon_2^- = \epsilon_2^+$ and $\eta_2^+ = \eta_2^-$ are comparable.

## 4 Matching with intermediate region

For every value of $r$, our aim is to suitably match the NH and far-away solutions in the intermediate era. We change the HG function factor $S$ in Eq. (19) with $1-S$ to expand the expression.

$$\begin{aligned}(R_{wlm})_{NH}(S) = (-S+1)^{\eta_1}\Bigg[&\frac{\Gamma(\bar{c}_1)\Gamma(\bar{c}_1-\bar{a}_1-\bar{b}_1)}{\Gamma(-\bar{a}_1+\bar{c}_1)\Gamma(\bar{c}_1-\bar{b}_1)}\\ &\times\hat{F}(\bar{a}_1,\bar{b}_1,\bar{c}_1;1-S)\\ &+(1-S)^{\bar{c}_1-\bar{a}_1-\bar{b}_1}\frac{\Gamma(\bar{c}_1)\Gamma(-\bar{c}_1+\bar{b}_1+\bar{a}_1)}{\Gamma(\bar{b}_1)\Gamma(\bar{a}_1)}\\ &\times\hat{F}(+\bar{c}_1-\bar{a}_1,+\bar{c}_1-\bar{b}_1,1-\bar{a}_1\\ &-\bar{b}_1+\bar{c}_1;1-S)\Bigg]\hat{A}_1 S^{\epsilon_1}. \end{aligned} \tag{23}$$

Through Eq. (13), we get

$$1-S = \frac{\frac{2M}{r} - \frac{\alpha M^2}{r^4}\left[1+\frac{\Lambda r^3}{6M}\right]^2}{1-\frac{\Lambda r^2}{3}}.$$

The horizon is computed as follows using a limiting value of $r \gg r_h$, $f(r)=0$, and a value of $M$ for $S \to 1$. This gives the stretched NH as

$$\begin{aligned}(1-S)^{\eta_1} &\simeq \left[\frac{r_h}{r}\frac{2r_h r^3 - r_h^3(r_h-1)}{\alpha_* r^3}\right]^{\eta_1}\\ &\simeq \left[\frac{r_h}{r}\frac{2r_h r^3 - r_h^3(r_h-1)}{\alpha_* r^3}\right]^{-l},\end{aligned}$$

and

$$\begin{aligned}(1-S)^{\eta_1-\bar{a}_1-\bar{b}_1+\bar{c}_1} &\simeq \left[\frac{r_h}{r}\frac{2r_h r^3 - r_h^3(r_h-1)}{\alpha_* r^3}\right]^{\eta_1}\\ &\simeq \left[\frac{r_h}{r}\frac{2r_h r^3 - r_h^3(r_h-1)}{\alpha_* r^3}\right]^{-\eta_1+A-B+1}\\ &\simeq \left[\frac{r_h}{r}\frac{2r_h r^3 - r_h^3(r_h-1)}{\alpha_* r^3}\right]^{1+l},\end{aligned}$$

with $\alpha_* = \frac{\alpha}{r_h}$, respectively. The NH solution in the intermediate domain is presented by

$$(R_{wlm})_{NH}(S) = \tilde{A}_1\left(\frac{r}{r_h}\right)^l + \tilde{A}_2\left(\frac{r}{r_h}\right)^{-(1+l)}, \tag{24}$$

with

$$\tilde{A}_1 = \hat{A}_1\left[\frac{2r_h r^3 - r_h^3(r_h-1)}{\alpha_* r^3}\right]^{-l}\frac{\Gamma(\bar{c}_1)\Gamma(-\bar{a}_1-\bar{b}_1+\bar{c}_1)}{\Gamma(\bar{c}_1-\bar{b}_1)\Gamma(\bar{c}_1-\bar{a}_1)},$$
$$\tilde{A}_2 = \hat{A}_1\left[\frac{2r_h r^3 - r_h^3(r_h-1)}{\alpha_* r^3}\right]^{1+l}\frac{\Gamma(\bar{a}_1+\bar{b}_1-\bar{c}_1)\Gamma(\bar{c}_1)}{\Gamma(\bar{a}_1)\Gamma(\bar{b}_1)}.$$

The HG function parameters are stretched by varying $T$ with $1-T$ and restricted for both lesser amounts of $\alpha$ and $\Lambda$ using $T(r_f) \to 0$. The BH event horizon has now been used to obtain the solution at a great distance. Thus, Eq. (20) yields

$$(1-T)^{\eta_2} \simeq \left[\frac{r_f}{r} - \frac{r_f}{r^3} + \frac{1}{r r_f}\right]^l,$$

and

$$(1-T)^{\eta_2+\bar{c}_2-\bar{a}_2-\bar{b}_2} \simeq \left[\frac{r_f}{r} - \frac{r_f}{r^3} + \frac{1}{r r_f}\right]^{1+l}\left(\frac{r}{r_f}\right)^{-(1+l)}.$$

The solution of Eq. (22) associated with the far-field horizon leads to

$$\begin{aligned}(R_{wlm})_f(T) = &\left(\tilde{H}_1\tilde{B}_1 + \tilde{H}_3\tilde{B}_2\right)\left(\frac{r}{r_f}\right)^l\\ &+\left(\tilde{H}_2\tilde{B}_1 + \tilde{B}_2\tilde{H}_4\right)\left(\frac{r}{r_f}\right)^{-(l+1)},\end{aligned} \tag{25}$$

where

$$\tilde{H}_1 = \frac{\Gamma(\bar{c}_2)\Gamma(\bar{c}_2-\bar{a}_2-\bar{b}_2)}{\Gamma(\bar{c}_2-\bar{a}_2)\Gamma(\bar{c}_2-\bar{b}_2)}\left[\frac{r_f}{r} - \frac{r_f}{r^3} + \frac{1}{r r_f}\right]^{-l},$$
$$\tilde{H}_2 = \frac{\Gamma(\bar{c}_2)\Gamma(-\bar{c}_2+\bar{b}_2+\bar{a}_2)}{\Gamma(\bar{b}_2)\Gamma(\bar{a}_2)}\left[\frac{r_f}{r} - \frac{r_f}{r^3} + \frac{1}{r r_f}\right]^{1+l},$$
$$\tilde{H}_3 = \frac{\Gamma(2-\bar{c}_2)\Gamma(\bar{c}_2-\bar{a}_2-\bar{b}_2)}{\Gamma(1-\bar{a}_2)\Gamma(1-\bar{b}_2)}\left[\frac{r_f}{r} - \frac{r_f}{r^3} + \frac{1}{r r_f}\right]^{-l},$$
$$\tilde{H}_4 = \frac{\Gamma(2-\bar{c}_2)\Gamma(\bar{a}_2+\bar{b}_2-\bar{c}_2)}{\Gamma(1+\bar{a}_2-\bar{c}_2)\Gamma(1+\bar{b}_2-\bar{c}_2)}\left[\frac{r_f}{r} - \frac{r_f}{r^3} + \frac{1}{r r_f}\right]^{l+1}.$$

Similar powers of $l$ and $l+1$ are used to compare the two asymptotic solutions as

$$\tilde{A}_1 = \tilde{H}_3\tilde{B}_2 + \tilde{H}_1\tilde{B}_1, \quad \tilde{A}_2 = \tilde{B}_1\tilde{H}_2 + \tilde{H}_4\tilde{B}_2.$$

Moreover, the constants of integration $\tilde{B}_1$ and $\tilde{B}_2$ are evaluated as

$$\tilde{B}_1 = \frac{\tilde{A}_1\tilde{H}_4 - \tilde{A}_2\tilde{H}_3}{\tilde{H}_1\tilde{H}_4 - \tilde{H}_2\tilde{H}_3} \quad \tilde{B}_2 = \frac{\tilde{A}_1\tilde{H}_2 - \tilde{A}_2\tilde{H}_1}{\tilde{H}_2\tilde{H}_3 - \tilde{H}_1\tilde{H}_4}.$$

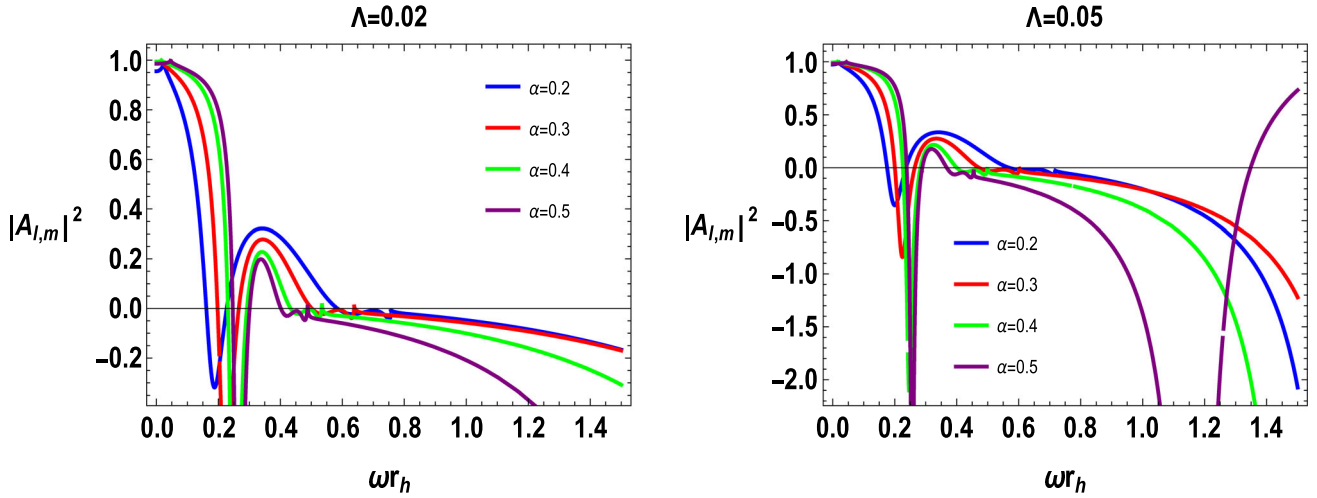


**Fig. 3** GBF versus $wr_h$ with different values of $\alpha$ and $\Lambda$ with $M = 0.5, l = 1$

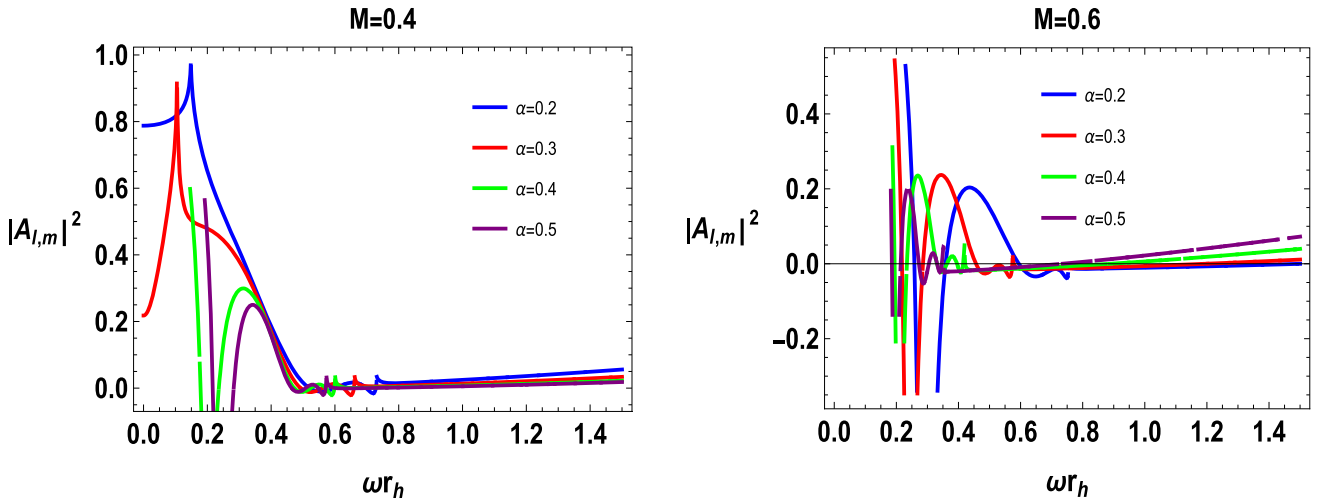


**Fig. 4** GBF versus $wr_h$ with different values of of $\alpha$ and $M$ with $l = 1, \Lambda = 0.02$

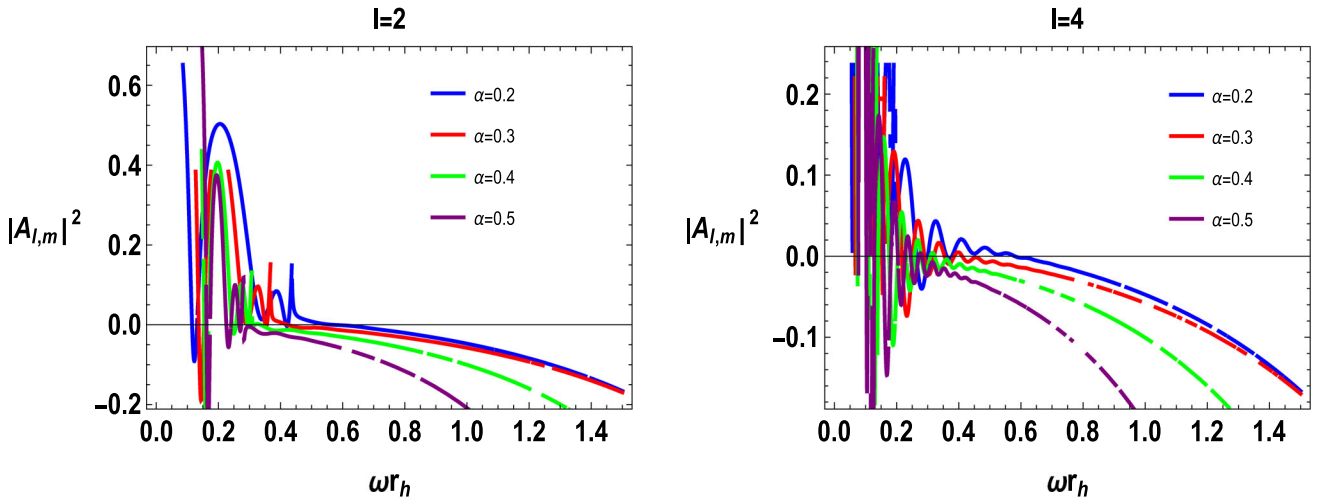


**Fig. 5** GBF versus $wr_h$ with different values of $\alpha$ and $l$ with $M = 0.5, \Lambda = 0.02$

The GBF can be formulated as given below to calculate the rate of emission associated with a massless scalar field.

$$|A_{l,m}|^2 = 1 - \left|\frac{\tilde{B}_2}{\tilde{B}_1}\right|^2 = 1 - \left|\frac{\tilde{A}_1\tilde{H}_2 - \tilde{A}_2\tilde{H}_1}{\tilde{A}_2\tilde{H}_3 - \tilde{A}_1\tilde{H}_4}\right|^2.$$

Visual analysis shows that waves go beyond the far cosmic horizon and beyond the event horizon. Waves of lower frequency are reflected whereas the waves of higher frequency are caught up, suggesting a relationship between the frequency of wave and emission rate. It should be noted that high-frequency waves have an easier time passing through obstructions. Through visual description, we investigate the effects of several physical factors on the GBF, which integrates the absorption probability and the emission rate of massless scalar fields. Waves that are located farther from the horizon pass against a filtering barrier that might let them cross or reflect. It is essential to comprehend how the frequency of the wave and effective potential interact in this filtering procedure. When the wave frequency is greater than the effective potential, it can pass through the barrier; For greater potential than the frequency, partial reflection and transmission occur, which lowers the GBF. This scenario can be examined under various situations to evaluate the numerical feasibility of the GBF. In contrast to reflection or transmission, a particle can enter a BH by absorption, as demonstrated by the GBF's scattering and absorption processes, which quantify the behavior of particles approaching a BH. Understanding this concept is essential for understanding the thermodynamic behavior of BHs, which is crucial for the study of BH geometry and quantum gravity in curved spacetime. Since the GBF measures the modification of radiation caused by potential barriers, it is crucial to comprehend the interactions between scalar fields and BH spacetime. We can learn more about the rate of emission energy as well as the information loss in the thermodynamics of BH by examining this aspect. Radial oscillations in the scalar field's absorption rate are shown in Figs. 3, 4 and 5.

The GBF $|A_{l,m}|^2$, which describes how BHs absorb and emit radiation under different conditions, especially as a function of the frequency $\omega$ and the BH horizon radius $r_h$, is depicted in the figures. We investigate the roles of the BH's mass (M), the cosmological constant $\Lambda$, the angular momentum, and the quantum parameter. Lower values of $\Lambda$ (e.g., $\Lambda = 0.02$) result in sharp peaks and troughs in the GBF for different $\alpha$ values, as shown in the Fig. 3. This suggests that higher quantum parameters improve absorption by increasing scattering at various frequencies. The total height of the GBF component falls as $\Lambda$ rises (e.g., $\Lambda = 0.05$), indicating that absorption characteristics have stabilized under the effect of dark energy. Variations in the BH's mass have a significant impact on the resonance structure, as the middle row demonstrates in Fig. 4. For example, at $M = 0.6$, the absorption curves exhibit more erratic behavior and pronounced low-energy absorption, indicating a more stable environment surrounding the massive BH. The influence of angular momentum is lastly demonstrated in Fig. 5, where sharper resonance peaks and a more complex interaction of radiation dynamics result from increases $l$.

The factor of particles of massless scalar extracted through a BH (particle flux) in connection with frequency and time is evaluated as

$$\begin{aligned}\frac{d^2\widetilde{P}}{dtdw} &= \sum_{l,m}|A_{l,m}|^2\frac{1}{2\pi e^{\frac{\kappa}{T_H}-1}}\\ &= \sum_{l,m}\left(1 - \left|\frac{\tilde{A}_1\tilde{H}_2 - \tilde{A}_2\tilde{H}_1}{\tilde{A}_2\tilde{H}_3 - \tilde{A}_1\tilde{H}_4}\right|^2\right)\frac{1}{2\pi e^{-1+\frac{\kappa}{T_H}}},\end{aligned}$$

and

$$\begin{aligned}\frac{d^2\widetilde{N}}{dtdw} &= \sum_{l,m}|A_{l,m}|^2\frac{w}{2\pi e^{\frac{\kappa}{T_H}-1}}\\ &= \sum_{l,m}\left(1 - \left|\frac{\tilde{A}_1\tilde{H}_2 - \tilde{A}_2\tilde{H}_1}{\tilde{A}_2\tilde{H}_3 - \tilde{A}_1\tilde{H}_4}\right|^2\right)\frac{w}{2\pi e^{-1+\frac{\kappa}{T_H}}}.\end{aligned}$$

Also, the expression for the angular momentum emission rate gradient can be displayed in a similar manner. Utilizing the following equation, the absorption cross-section of any partial wave can be determined.

$$\sigma = \sum_{l,m}\frac{\pi}{w^2}|A_{l,m}|^2 = \sum_{l,m}\frac{\pi}{w^2}\left(1 - \left|\frac{\tilde{A}_1\tilde{H}_2 - \tilde{A}_2\tilde{H}_1}{\tilde{A}_2\tilde{H}_3 - \tilde{A}_1\tilde{H}_4}\right|^2\right).$$

## 5 Concluding remarks

In this study, we derived an analytical expression for the GBF in the quantum Oppenheimer–Snyder–dS spacetime. By solving the radial equation of motion near both the event and cosmological horizons and connecting the asymptotic solutions through a matched intermediate region, we obtained an expression for the GBF in terms of hypergeometric functions. This allowed us to compute the energy emission rate and absorption cross-section for massless scalar fields, offering new insights into the quantum behavior of radiation in curved backgrounds.

We thoroughly examined the behavior of the effective potential, which governs scalar wave propagation in the BH spacetime. As depicted in Figs. 1 and 2, the effective potential exhibits clear dependence on key physical parameters such as the quantum parameter $\alpha$, BH mass $M$, and angular momentum $l$.

- Specifically, lower values of $\alpha$ lead to higher and narrower potential barriers (Fig. 1), enhancing wave reflection and reducing transmission. Conversely, increasing the BH mass diminishes the peak height of the potential,

making it easier for waves especially low energy modes to tunnel through.
- Additionally, as shown in Fig. 2, greater angular momentum amplifies the effective potential, producing a stronger centrifugal barrier that predominantly affects low-frequency radiation. These trends confirm that the quantum parameter plays a dominant role in shaping the effective potential, thus influencing the wave absorption characteristics of spacetime.

We also investigated the GBF $|A_{l,m}|^2$, which quantifies deviations from ideal blackbody emission, by exploring its sensitivity to spacetime parameters and wave properties. Our analysis reveals that the GBF is highly sensitive to variations in the BH's mass $M$, the cosmological constant $\Lambda$, angular momentum $l$, and the quantum parameter $\alpha$. These parameters significantly influence the effective potential, and hence, the absorption probability. Figures 3 and 5 illustrate how the GBF varies with frequency $\omega$, quantum factor $\alpha$, BH mass $M$, cosmological constant $\Lambda$, and angular momentum $l$.

- In Fig. 3, the GBF is plotted for two values of the cosmological constant: $\Lambda = 0.02$ (left) and $\Lambda = 0.05$ (right), with fixed $M = 0.5$ and $l = 1$. We observe that at lower $\Lambda$, sharper oscillations and resonance structures appear for different $\alpha$, especially at lower frequencies. This suggests stronger frequency-dependent scattering in the presence of a weaker cosmological constant. As $\Lambda$ increases, the curves become smoother and less pronounced, indicating that dark energy suppresses absorption fluctuations, stabilizing the GBF spectrum across frequencies.
- Figure 4 examines the impact of varying BH mass $M = 0.4$ (left) and $M = 0.6$ (right), again for $l = 1$ and $\Lambda = 0.02$. At smaller $M$, the GBF decays more quickly with increasing frequency and shows more noticeable suppression at low frequency, especially for higher $\alpha$. In contrast, for larger mass $M = 0.6$, the GBF displays more complex oscillatory patterns, with enhanced absorption at low frequencies and a broader spectrum of transmission. This indicates that larger BHs enhance low-frequency absorption, owing to a deeper potential well and broader interaction region for incoming waves.
- In Fig. 5, the role of angular momentum is highlighted with $l = 2$ (left) and $l = 4$ (right), while keeping $M = 0.5$ and $\Lambda = 0.02$. As $l$ increases, the GBF spectrum shifts downward, and resonance peaks become more sharply defined. This behavior reflects the growing influence of the centrifugal barrier, which inhibits low-energy wave penetration for higher angular momentum modes. Accordingly, the transmission probability reduces significantly at higher $l$, emphasizing that angular momentum acts as a filter for low-frequency modes in scalar field scattering.

In summary, our analysis elucidates how quantum corrections and BH parameters intricately control both the effective potential landscape and the greybody spectrum. The results significantly enhance our understanding of quantum field behavior in curved spacetime, particularly the influence of mass, dark energy, angular momentum, and quantum parameters on wave scattering and energy emission. This work sets a robust foundation for further studies on quantum radiation processes and their implications in modified gravity and BH thermodynamics.

**Data Availability Statement** My manuscript has no associated data. [Authors' comment: This is a theoretical study and no experimental data is included.]

**Code Availability Statement** My manuscript has no associated code/software. [Authors' comment: No numerical calculations are performed, hence no code/software is used.]


Funded by SCOAP[3].

## References

1. J.D. Bekenstein, Lett. Nuovo Cim. **4**, 737 (1972)
2. J. Lewandowski, Y. Ma, J. Yang, C. Zhang, Phys. Rev. Lett. **130**, 101501 (2023)
3. J. Lin, X. Zhang, Phys. Rev. D **110**, 026002 (2024)
4. C. Zhang, Y. Ma, J. Yang, Phys. Rev. D **108**, 104004 (2023)
5. C.-Y. Shao, C. Zhang, W. Zhang, C.-G. Shao, Phys. Rev. D **109**, 064012 (2024)
6. D. Lombardo, Class. Quantum Gravity **21**, 1407 (2004)
7. S. Luo, C. Li, Phys. Rev. D **110**, 124042 (2024)
8. F. Javed, A. Waseem, B. Almutairi, Eur. Phys. J. C **83**(9), 811 (2023)
9. G. Mustafa et al., Ann. Phys. **460**, 169551 (2024)
10. F. Javed, Phys. Dark Univ. **44**, 101450 (2024)
11. G. Fatima et al., Phys. Dark Univ. **45**, 101521 (2024)
12. G. Mustafa et al., Phys. Dark Univ. **45**, 101508 (2024)
13. F. Javed, M.H. Alshehri, Ann. Phys. **464**, 169658 (2024)
14. G. Murtaza et al., J. High Energy Astrophys. **44**, 279–289 (2024)
15. A. Ditta et al., Phys. Dark Univ. **47**, 101818 (2025)
16. G. Mustafa et al., Phys. Dark Univ. **46**, 101708 (2024)
17. S.W. Hawking, Commun. Math. Phys. **43**, 199 (1975)
18. R.M. Wald, Living Rev. Relativ. **4**, 6 (2001)

19. I. Georgescu, Nat. Rev. Phys. **4**, 7 (2022)
20. J.D. Bekenstein, Phys. Rev. D **7**, 2333 (1973)
21. J.M. Bardeen, B. Carter, S.W. Hawking, Commun. Math. Phys. **31**, 161 (1973)
22. S.W. Hawking, Commun. Math. Phys. **43**, 199 (1975)
23. S.W. Hawking, D.N. Page, Commun. Math. Phys. **87**, 577 (1983)
24. R.M. Wald, Living Rev. Relativ. **4**, 6 (2001)
25. D.N. Page, New J. Phys. **7**, 203 (2005)
26. H. Nastase, arXiv:2112.01234
27. D. Kastor, S. Ray, J. Traschen, Class. Quantum Gravity **26**, 195011 (2009)
28. D. Kastor, S. Ray, J. Traschen, Class. Quantum Gravity **27**, 235014 (2010)
29. D. Kastor, S. Ray, J. Traschen, Class. Quantum Gravity **28**, 195022 (2011)
30. D. Kastor, S. Ray, J. Traschen, Class. Quantum Gravity **36**, 024002 (2018)
31. S.H. Hendi, M. Vahidinia, Phys. Rev. D **88**, 084045 (2013)
32. A.M. Frassino, D. Kubizunak, R.B. Mann, F. Simovic, JHEP **80**, 2014 (2014)
33. D. Kubiznak, B.R. Mann, JHEP **07**, 033 (2012)
34. A. Belhaj, M. Chabab, H. El Moumni, M.B. Sedra, Chin. Phys. Lett. **29**, 100401 (2012)
35. S.H. Hendi, B. Eslam Panah, S. Panahiyan, Phys. Lett. B **769**, 191 (2017)
36. J. Maldacena, Int. J. Theor. Phys. **38**, 1113 (1999)
37. L.H. Ford, Phys. Rev. D **12**, 2963 (1975)
38. S.S. Gubserv, I.R. Klebanov, Phys. Rev. Lett. **77**, 4491 (1996)
39. J.M. Maldacena, A. Strominger, Phys. Rev. D **55**, 861 (1997)
40. I.R. Klebanov, S.D. Mathur, Nucl. Phys. B **500**, 115 (1997)
41. W.T. Kim, J.J. Oh, Phys. Lett. B **461**, 189 (1999)
42. E. Berti, V. Cardoso, M. Casals, Phys. Rev. D **73**(024013), 109902 (2006)
43. C. Flammer, *Spheroidal Wave Functions* (Stanford University Press, Redwood City, 1957)